Clays and Clay Minerals, Vol. 63, No. 6, 457–468, 2015.

EFFECT OF SURFACE CHARGE AND ELEMENTAL COMPOSITION ON THE SWELLING AND DELAMINATION OF MONTMORILLONITE NANOCLAYS USING SEDIMENTATION FIELD-FLOW FRACTIONATION AND MASS SPECTROSCOPY

Shoeleh Assemi[1,*], Sugandha Sharma[1], Soheyl Tadjiki[2], Keith Prisbrey[1], James Ranville[3], and Jan D. Miller[1]

[1] Department of Metallurgical Engineering, University of Utah, Salt Lake City, Utah, USA
[2] Postnova Analytics USA, Salt Lake City, Utah, USA
[3] Department of Chemistry, Colorado School of Mines, Golden, Colorado, USA

Abstract—The swelling properties of smectite-type clay particles (including montmorillonite) are of interest in various industries. A fundamental understanding of the surface properties of smectite particles at the sub-micron level would facilitate investigation of the effect of distributed properties such as charge and elemental composition. Swelling and delamination of SWy-2 Na-montmorillonite (Na-Mnt) nano-clay particles were studied here using size distributions obtained by sedimentation field-flow fractionation (SdFFF). Fractions were examined by electron microscopy and inductively-coupled optical emission spectroscopy (ICP-OES). Two distinct populations were observed in the size distribution of SWy-2 Na-Mnt particles (bimodal size distribution), with mean equivalent spherical diameters of ~60 nm and 250 nm, respectively. In contrast, the size distribution of STx-1 Ca-montmorillonite (Ca-Mnt) particles showed only one peak with a mean equivalent spherical diameter of ~410 nm, which changed to 440 nm after 4 days of hydration. Analyses of the fractions by ICP-OES obtained along the size distribution of Na-Mnt showed an abundance of Ca and Mg in the fractions below 250 nm, and confirmed the presence of Fe and Mg as isomorphous substituents. Electron micrographs of the fractions obtained from Na-Mnt size distributions were used to calculate the thickness of the clay particles. Bridging forces between pure or Mg-substituted montmorillonite and either Ca^{2+} or Na^{+} were calculated using semi-empirical methods. The results demonstrated that swelling and delamination of Na-Mnt clay particles are dictated by properties such as elemental composition and surface charge which are distributed along the size distribution.

Key Words—Ca-montmorillonite, Delamination, Molecular dynamics Simulation, Na-montmorillonite, Optical Emission Spectroscopy, Particle Thickness, Sedimentation Field-flow Fractionation, Swelling.

INTRODUCTION

Smectite-type clays (including montmorillonite) are used extensively in industrial applications such as in oil-well drilling mud and fillers, in civil and environmental engineering for plugging leaks in soil, rocks, and dams, and in cosmetics, nano-structured clay polymer composites, and clay hydrogels. The swelling properties of smectites can be undesirable. For example, in the drilling industry and especially in oil and gas exploration, smectites in the sedimentary rocks can potentially lead to wellbore collapse. Smectite clays may also stick to drill bits, and in some cases the clay sticking and "balling" can result in drill-bit loss (Anderson *et al.*, 2010).

An understanding of the underlying microscopic mechanisms is the key to controlling clay swelling. Modeling and molecular dynamics simulation studies suggest that the interaction of interlayer particles with water molecules influence clay-swelling properties (Chiou and Rutherford, 1997; Low, 1980). Such interactions would stem from the hydration ability of particular ions, and, in turn, the surface-charge properties of the clay particles. This valuable information is mainly hidden in the smallest clay particles but clay properties at sub-micron levels have been poorly studied. The motivation for the present study was to test the hypothesis that the surface charge of clay particles is a distributed property and that this charge characteristic will influence the swelling characteristic of smectite particles. A separation technique was used to obtain narrow fractions of smectite clay particles. The surface charge and elemental composition of the Na-montmorillonite (Na-Mnt) clay particles as a function of size were then used to form a fundamental understanding of its swelling phenomena at the sub-micron level.

Almost all clay structures can hydrate. One to four layers of water molecules can line up in a stepwise mechanism to form a quasi-crystalline structure between unit layers which can result in an increase of 9−20 Å in the interlayer space (crystalline swelling) (Laird, 2006; Anderson *et al.*, 2010). Some smectite clays (*e.g.* Na- or Li-montmorillonite) can swell to dimensions several

* E-mail address of corresponding author:
Shoeleh.Assemi@utah.edu
DOI: 10.1346/CCMN.2015.0630604

times the clay-layer thickness as a result of the hydration of the exchangeable cations covering the clay interlayers (Boek *et al.*, 1995).

Common monovalent cations hydrate in the order: $Li^+ > Na^+ > K^+ > NH_4^+ > Cs^+$ (Hendricks *et al.*, 1940). The degree of hydration decreases as the cation size increases. Divalent and large monovalent cations shield the charge of the interlayer and thus reduce the hydration (Norrish, 1954). If the concentration of the interlayer cations is greater than that of the surrounding water, the water molecules will be drawn between the clay interlayers to screen the cation charge. This is called osmotic swelling and can result in interlayer spacing of 20–130 Å, and in many cases, delamination of the clay particles. These delaminated layers have been observed along with the larger clay particles in several imaging studies of Na-Mnt clays (Michot *et al.*, 2004; Cadene *et al.*, 2005).

Greater water retention was observed for high-charge compared to low-charge smectites (Chiou and Rutherford, 1997; Low, 1980) whereas Viani *et al.* (1983) reported little or no effect of surface-charge density on clay swelling for eight Na-smectites. The variation could be a result of the difference in clay-mineral composition rather than the layer charge, according to Laird (1999), because the increase in cation charge should shield the charges on the interlayers and decrease the swelling. Experiments by Laird (1999) on 2:1 phyllosilicates showed an increase in hydration with an increase in the accessible surface area, but found mostly a random relationship between the layer charge and the adsorbed-water content. Such results might be due to slight differences in the charge of the clay particles which may not have been detected during the measurement of the bulk sample. In fact, surface charge is expected to be a distributed property. Not all of the particles for a given smectite will have the same surface-charge density. Although successful attempts have been made to measure the surface charge of individual clay particles (Liu *et al.*, 2014), direct measurements of the layer charges of particles of different sizes have not yet been reported.

Most investigations of clay minerals have been performed on bulk samples with a broad size distribution, but the size dependence of clay-surface properties has always been recognized. Some differences in charge or swelling behavior of clay samples fractionated by centrifugation have been reported (Katti and Shanmugasundaram, 2001) but concerns were expressed about the possibility of cations being washed during the centrifugation process (Roberson *et al.*, 1968).

The utility of field-flow fractionation (FFF) sub-techniques for fractionation and analysis of clay particles is well documented (Beckett *et al.*, 1992; Taylor *et al.*, 1992). Correlation of specific ions with the clay-mineral structure, as well as changes in mineralogy as a function of size, can be tracked by FFF, coupled with inductively coupled plasma-mass spectrometry (FFF-ICP-MS) techniques (Beckett *et al.*, 1992; v.d. Kammer *et al.*, 2004; Ranville *et al.*, 2005). The majority of FFF-ICP-MS analyses have been performed for kaolinite and illite clay particles or aquatic colloids. Characterization of bentonite samples using flow field-flow fractionation (FlFFF) have been hindered by sample loss due to sample–membrane interactions (Bouby *et al.*, 2008) as well as Al and Si leachates from the frit embedded in the FlFFF channel (Plaschke *et al.*, 2001). Such problems are minimal in sedimentation field-flow fractionation (SdFFF) where membranes and frits are not used.

In the present study, clay-sample fractions obtained along the clay-size distributions were analyzed for charge and elemental composition. Combination of these data with the particle mass obtained from SdFFF and projected area from electron microscopy (two fractions) provided interesting information about delamination, swelling, and aggregation occurring upon hydration of Na-Mnt particles. A characteristic bimodal size distribution obtained for Na-Mnt demonstrated that size distribution can be used as a quick marker for identification of swelling clays.

Here SdFFF elution profiles (fractograms) of Na-Mnt and Ca-Mnt (Ca-montmorillonite), as well as the analyses of the Na-Mnt fractions for surface charge and elemental composition, are presented. Electron micrographs of the fractions obtained were used to estimate the thickness of primary (delaminated) and aggregated clay-particle populations. Molecular-dynamics simulations were used to further describe the observed delamination behavior of Na-Mnt.

MATERIALS AND METHODS

Clay samples

The Na-rich montmorillonite (Na-Mnt) used in the present study was from Crook County, Wyoming, USA (SWy-2) and the Ca-rich montmorillonite (Ca-Mnt) was from Gonzales County, Texas, USA (STx-1). Both clays were purchased from the Source Clays Repository of The Clay Minerals Society and were used in their natural states without prior treatment. The structural formula for SWy-2 Na-Mnt is reported as $(Ca_{0.12}Na_{0.32}K_{0.05})[Al_{3.01}Fe(III)_{0.41}Mn_{0.01}Mg_{0.54}Ti_{0.02}][Si_{7.98}Al_{0.02}]O_{20}(OH)_4$ and that for STx-1 Ca-Mnt, as $(Ca_{0.27}Na_{0.04}K_{0.1})[Al_{2.41}Fe(III)_{0.09}Mg_{0.71}Ti_{0.03}][Si_{8.00}]O_{20}(OH)_4$ (Mermut and Cano, 2001). Cation exchange capacities for SWy-2 Na-Mnt and STx-1 Ca-Mnt were reported as 84 and 89 meq/100 mg, respectively (Borden and Giese, 2001). A suspension of each clay (5 mg/mL) was prepared in polycarbonate tubes using deionized water (Academic Unit, Millipore, Billerica, Massachusetts, USA). The pH values for the suspensions were measured as 8.6 for SWy-2 and 7.7 for STx-1, which remained constant during the course of the experiments

https://doi.org/10.1346/CCMN.2015.0630604 Published online by Cambridge University Press

(data not shown). Electrophoretic mobilities (EPM) of the clay fractions were measured using laser doppler velocimetry (Brookhaven ZetaPALS, Holtsville, New York, USA). Electron micrographs of the clay fractions were obtained using a Tecnai T12 transmission electron microscope (FEI, Hillsboro, Oregon, USA), located at the University of Utah Core Facilities. Approximately 5 μL of the sample suspension was air dried on a formvar carbon-coated copper grid (Electron Microscopy Science, Hatfield, Pennsylvania, USA). The samples were mounted in the electron microscope using the Tecnai T12 standard sample holder. A bright-field imaging mode was used with a spot size of 2. The emitter was a LaB_6 filament. The gun vacuum was 8.83×10^{-8} torr, and a beam accelerating voltage of 120 kV was employed. The electron micrographs obtained were analyzed using *ImageJ* software (Schneider *et al.*, 2012).

Sedimentation field-flow fractionation

Sedimentation field-flow fractionation experiments were performed using a Postnova S101 centrifugal FFF unit, with ultraviolet (UV) detection at 254 nm (Shimadzu, Duisburg, Germany). The UV detection at 254 nm for clay particles has been attributed to scattering rather than absorption (Taylor *et al.*, 1992). Field-decay programming was used to reduce the run time. The applied initial fields were 1000 rpm for STx-1 Ca-Mnt and 2000 rpm for SWy-2 Na-Mnt, respectively. The injection volume was 100 μL for both samples. 0.05% Fisherbrand FL-70, a mixture of anionic and non-ionic surfactants (Fisher Scientific, Pittsburgh Pennsylvania, USA), was used as the carrier liquid with a channel flow rate of 1 mL/min. The carrier liquid was 1×10^{-4} M NaOH when fractions were collected for surface-charge analysis. The fractograms obtained in both carrier liquids showed no significant differences. Fractions were collected manually at set intervals. The fractograms were converted to size distributions using the FFF Analysis program (Postnova Analytics, Salt Lake City, Utah, USA).

Details of the principles of field-flow fractionation techniques can be found elsewhere (Giddings, 1993; Tadjiki *et al.*, 2009). Briefly, in FFF the separation takes place in a thin, flat channel by applying an external physical force to the sample species, to push the sample particles toward the lower channel wall (the accumulation wall). After a short 'relaxation time,' which allows for the equilibration of the sample species under the incoming field force and upward diffusion motion, the channel flow is initiated. The smaller sample species will elute first and the larger sample species will elute later. In SdFFF the centrifugal force is applied for separation and the particles are separated based on their buoyant mass. The sample elution time (t_r), sometimes referred to as the retention time, is approximately proportional to the particle mass in SdFFF (Beckett *et al.*, 1992; Giddings, 1993):

$$t_r \approx \frac{m(\Delta\rho/\rho_p)Gwt^0}{6kT} \quad (1)$$

where m is the particle mass, $\Delta\rho$ is the difference in the density between the sample species and the carrier, ρ_p is the particle density, G is the acceleration, w is the channel thickness (136 μm for the SdFFF channel used in the present study), t^0 is the elution time for non-retained particles, and kT is the kinetic energy (Boltzmann's constant × absolute temperature). For a constant applied field, the particle equivalent spherical diameter (d) can be calculated directly from the sample elution time:

$$d = \left(\frac{36kTt_r}{t^0\pi|\Delta\rho|Gw}\right)^{\frac{1}{3}} \quad (2)$$

In practice, to reduce the run time, the applied field is reduced using an exponential decay algorithm (Williams *et al.*, 2001).

SdFFF is an elution technique which allows for the fractions to be collected from the particle-size distribution. Assuming a constant sample density within a collected fraction, the mean particle thickness (t_p) can be calculated from the projected area (A_p) as determined using electron microscopy (Beckett and Giddings, 1997);

$$t_p \approx \frac{kT}{A_p\Delta\rho Gw\lambda} \quad (3)$$

where λ is the particle retention parameter. For well resolved peaks λ can be approximated as $\lambda \approx t^0/6t_r$, where t_r is the peak maximum for the particle and t^0 is the void peak, meaning the peak representing the particles that could not have been retained by the applied field (Giddings, 1993). In FFF, the particle elution is represented by a fractogram, which is a plot of the mass concentration of the particles *vs.* the elution time (t_r). The particle mass concentration is usually detected by a UV detector response, per unit of elution volume (dUV/dV_r), at a set wavelength. Size distributions in SdFFF are depicted by a plot of the relative mass which is defined as the change in cumulative mass eluted from the FFF channel per change in size (dm^c/dd) *vs.* the equivalent spherical diameter.

ICP-OES elemental analysis

For elemental analysis, the Na-Mnt minerals were prepared in the same manner as described above and were fractionated using a Postnova Analytics centrifugal FFF CF2000 instrument (Salt Lake City, Utah, USA). Fractions were obtained every 5 min (~5 mL in volume) and were analyzed using an Optima 5300 ICP-OES Spectrometer (Perkin Elmer, Woodbridge, Connecticut, USA) at the Department of Chemistry, Colorado School of Mines, Golden, Colorado, USA. The plasma conditions were as follows: RF power – 1500 W, plasma flow

https://doi.org/10.1346/CCMN.2015.0630604 Published online by Cambridge University Press

– 15 L/min, auxiliary gas flow – 0.5 L/min, and nebulizer gas flow – 0.8 L/min. Sample introduction (1 mL/min) was by means of a Meinhhard nebulizer and cyclonic spray chamber. The instrument was calibrated using multi-element standards and quality assurance samples (Fisher Scientific, Pittsburgh, Pennsylvania, USA), which included initial analysis of two Certified Check standards (High Purity Standards: Cat. # CCV-1 Solution A, Cat. # CCV-1 Solution B), nitric acid blanks (Fisher Scientific trace element grade), and a standard reference natural water sample (NIST 1640a, National Institute of Standards and Technology [NIST], Gaithersburg, Maryland, USA). Quality-assurance (QA) samples were analyzed after every ten samples. Instrumental drift was corrected by using continuous addition of a scandium internal standard. Using the elemental concentration in each fraction and the mean retention time for the collected fractions, the element-based size distributions were plotted as described by Taylor *et al*. (1992).

Quantum and molecular dynamics calculations

A montmorillonite primitive cell (from the *American Mineralogist* Crystal Structure database, Mineralogical Society of America, http://rruff.geo.arizona.edu/AMS/amcsd.php) was used for quantum calculations with *Mopac* at the PM7 level (Stewart, 2012). Solving the Schrödinger equation ($H\Psi = E\Psi$) gave energies (E), forces ($F = \partial E/\partial r$), and Mulliken charges of each nucleus. Intercalated Ca^{2+} and Na^{+} were compared by summing the forces between each cation and the surrounding tetrahedral layers.

In addition, molecular dynamics simulations were used to compare the effect of Ca^{2+} *vs*. Na^{+} on montmorillonite swelling. The steps were as follows: (1) the *Avogadro* program (Hanwell *et al.*, 2012) was used to create a multi-cell montmorillonite structure in *mol2* format. This format allowed inclusion of the Mulliken charges from above. (2) The montmorillonite structure was surrounded by explicit water (discrete water molecules) and *Amber*-style topology files were created using the *tleap* program (Gotz *et al.*, 2012) with *GAFF* and *ClayFF* force fields. (3) Finally, *amber2-lammps.py* (Novik, 2000) was used to convert the above files for use with *Lammps* (Plimpton, 1995), which allowed for preservation of the montmorillonite crystal structure during hydration and swelling.

RESULTS

A bimodal distribution was observed for the fractograms of the Na-Mnt sample injected immediately after preparation and after 4 days of equilibrium in solution (Figure 1a). For the sample injected immediately after preparation, a small peak was observed at ~12 min, followed by a larger peak appearing at ~42 min. After four days of equilibration, the intensity of the former peak increased significantly and it eluted at ~10 min. The intensity of the second peak decreased and it eluted at ~48 min.

The fractograms of Ca-Mnt (Figure 1b) showed only one peak, with a maximum at ~37 min for the fresh sample. After 4 days, this peak shifted to ~40 min.

The differential and cumulative size distributions for Na-Mnt and Ca-Mnt samples (Figure 2) showed peak maxima for two sample populations of the fresh Na-montmorillonite at 60 nm and 250 nm, respectively. After 4 days, the peak maxima shifted to 52 nm and 350 nm. The peak mean for the fresh Ca-Mnt sample was at 410 nm, which shifted to 440 nm after 4 days of hydration.

The EPM of the fractions obtained from the Na-Mnt particle-size distribution (Figure 3) showed that smaller particles carried a more positive charge, and the charge reached a plateau at ~200 nm.

The molar concentration of Al and Si in Na-Mnt followed the particle-size distribution (Figure 4). The Si/Al ratio was constant for smaller particles but showed some increase for particles with d >300 nm (Figure 5). The Ca/Al ratio decreased sharply as the particle size increased. The Mg/Al ratio was greater in the smaller size fractions and remained constant for particles with d >300 nm. The Fe/Al ratio was almost constant throughout the size distribution.

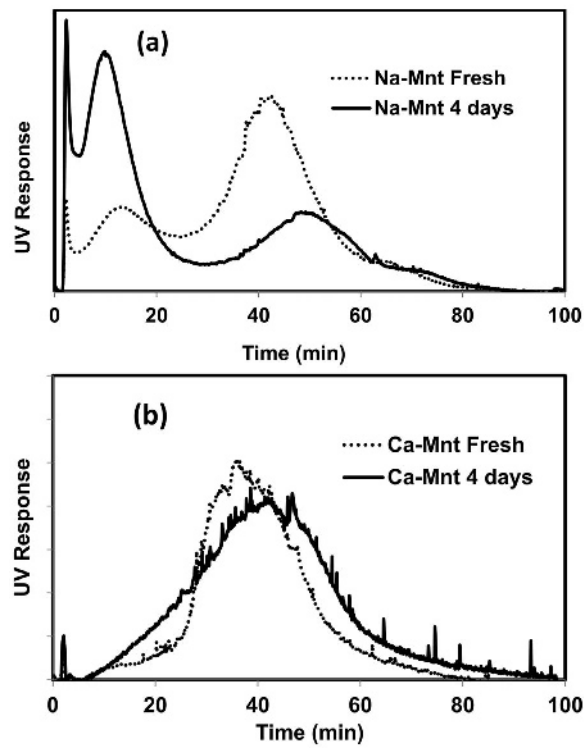

Figure 1. SdFFF elution profiles (fractograms) of (a) Na-Mnt and (b) Ca-Mnt clays immediately after preparation, and after 4 days of hydration.

https://doi.org/10.1346/CCMN.2015.0630604 Published online by Cambridge University Press

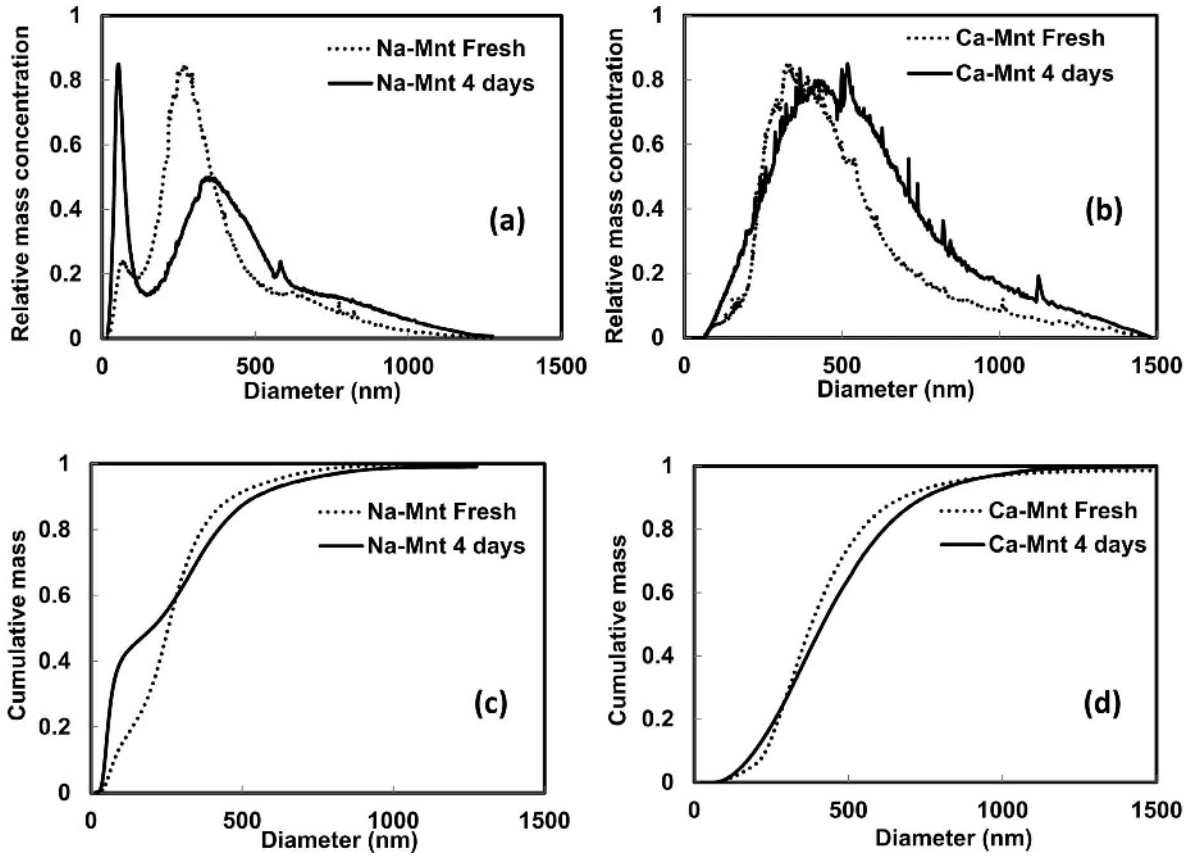

Figure 2. Differential (a,c) and cumulative (b,d) size distributions of Na-Mnt and Ca-Mnt clays immediately after preparation, and after 4 days of hydration. The relative mass represents the mass of the clay in the size range. A density of 2.6 g/mL was assumed for both the Na-Mnt and Ca-Mnt clay particles.

Electron micrographs (Figure 6) corresponding to the first elution peak of Na-Mnt (fraction collected at 13 min) showed transparent clay particles. Using equation 3, the average thickness of these particles was calculated as 2.6 nm. Micrographs obtained from the fraction collected at 38 minutes showed denser (darker) particles, with a calculated average thickness of ~36 nm (Table 1).

Preliminary molecular dynamics simulation (MDS) studies were used to mimic the swelling behavior of Na-Mnt, assuming that Mg^{2+} was only present in the crystal structure and Na^{+} or Ca^{2+} was present as the counter ion on the basal plane.

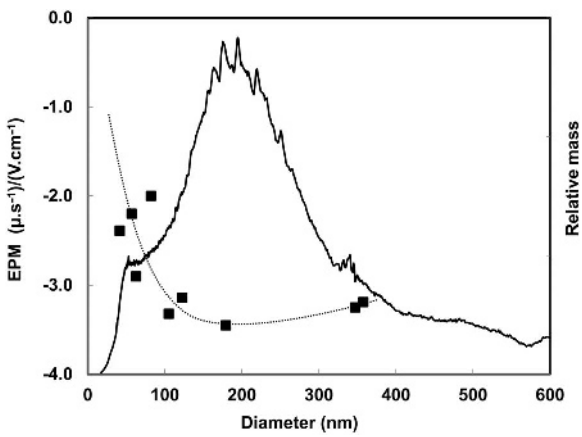

Figure 3. Electrophoretic mobility of Na-Mnt particles as a function of particle size, in deionized water, pH ≈ 8.6 (dotted line) shown with relative mass concentration (solid line).

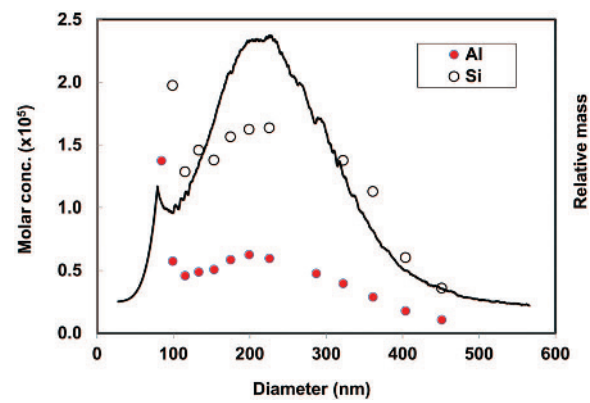

Figure 4. Elemental distributions of Al and Si in Na-Mnt and comparison with the UV trace.

https://doi.org/10.1346/CCMN.2015.0630604 Published online by Cambridge University Press

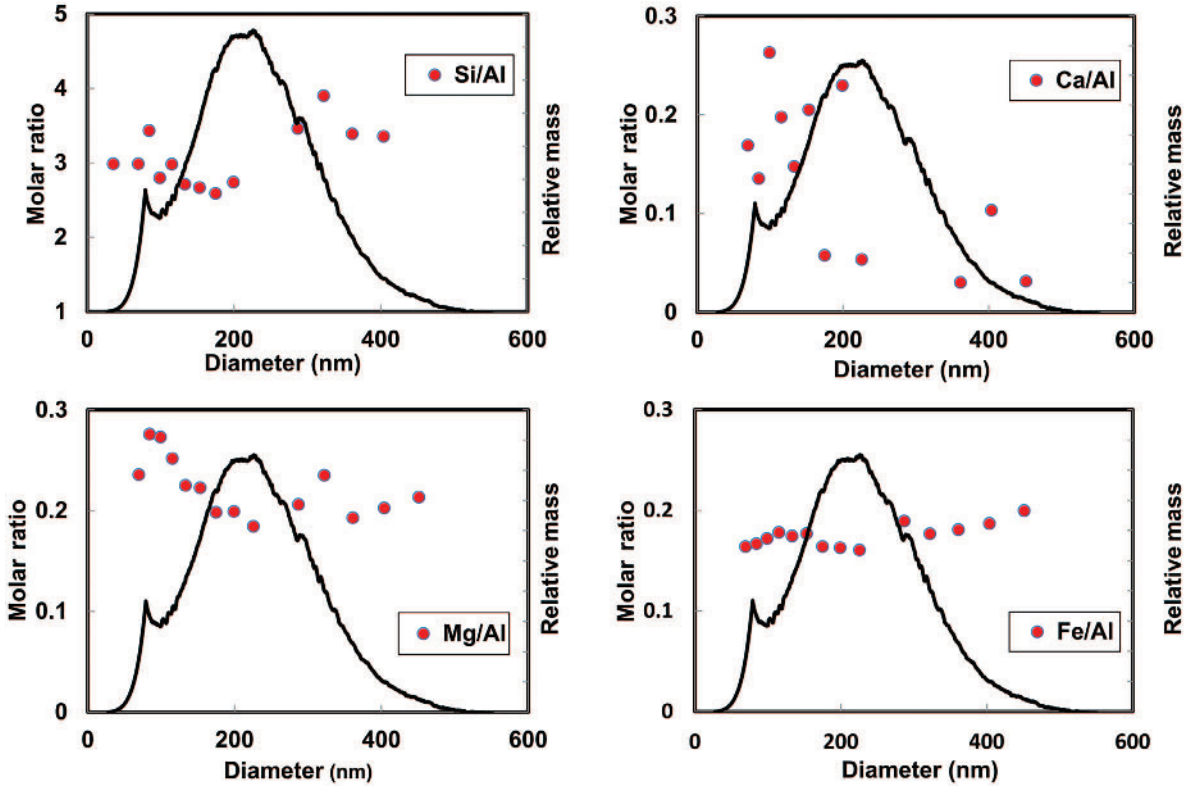

Figure 5. Molar ratios of Si, Ca, Mg, and Fe to Al, in Na-Mnt.

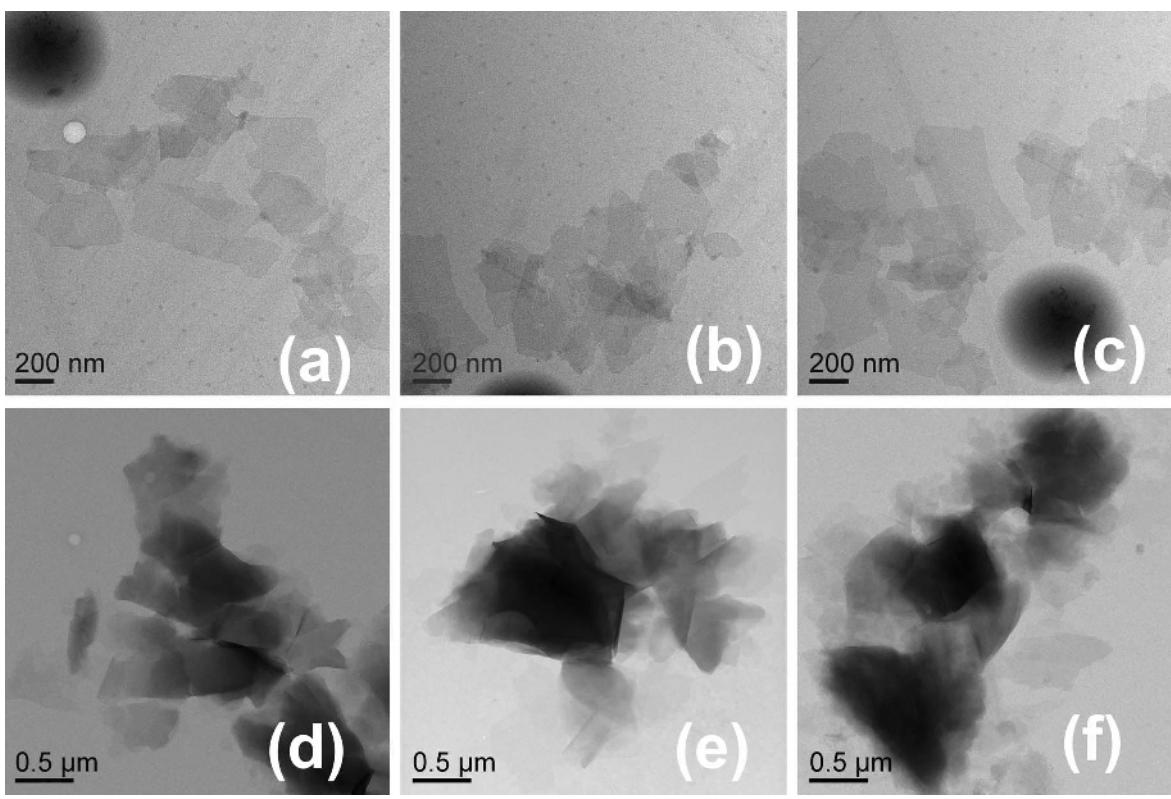

Figure 6. Electron micrographs of Na-Mnt fractions collected at 13 min (a,b,c) and 38 minutes (d,e,f).

https://doi.org/10.1346/CCMN.2015.0630604 Published online by Cambridge University Press

Table 1. Layer parameters calculated for the Na-montmorillonite fractions. The area was measured from the electromicrograph images.

Fraction time	Number of particle images (n)	Area ($\times 10^{13}$ m^2)	d_c ($\times 10^9$ m)	t_p ($\times 10^9$ m)	Number of stacked plates*
13 min	25	1.3 ± 0.7	410 ± 100	2.6 ± 1.1	1
38 min	15	1.8 ± 0.7	470 ± 100	35.9 ± 1.5	14

* assuming a thickness of 2.6 nm for the primary particles.
n is the number of particles measured, d_c is the particle equivalent disc diameter as determined by SdFFF, and t_p is the particle thickness calculated from equation 3.

Layers of montmorillonite were formed in explicit water with either Na^+ or Ca^{2+} ions in the interlayer spacing. Water molecules were expected to coordinate to Ca^{2+} or Na^+ ions. Instead, after a few femtoseconds, the Na^+ ions left the interlayer space, while the Ca^{2+} ions bridged the layers together (see the movie deposited with the Editor in Chief at: http://www.clays.org/JOURNAL/JournalDeposits.html).

Bridging forces between Ca^{2+} or Na^+ cations and the surface of the montmorillonite unit cell (Table 2) were calculated as the sum of Schrödinger equation-energies between individual atoms. The calculated bridging energy between Ca^{2+} ions and the montmorillonite surface was almost twice that of the Na^+ ions and the montmorillonite surface. Substitution of Mg^{2+} in the crystal did not change this proportion (a ratio of 0.2, taken from Figure 5, was used for Mg/Al).

DISCUSSION

In SdFFF, the separation is based on the particles' buoyant mass. The elution profile (fractogram) is presented by plotting the detector signal *vs.* retention time. The detector signal (in the present case, the UV signal at 254 nm) represents the mass concentration of the particles in the eluted segment. A change in the retention time (horizontal axis) reflects a change in the particle buoyant mass, and a change in the UV detector signal (vertical axis) represents a change in the mass concentration of the particle eluted at that specific time.

The fractogram obtained for Na-Mnt (Figure 1a) suggested the presence of two major fractions. One fraction represented a smaller size that decreased in buoyant mass (lower retention time) but increased in mass concentration (larger UV signal) upon hydration, and the other fraction represented a larger size (larger retention time) that increased by mass and size, and decreased by number, upon hydration. This bimodal behavior was absent from the fractograms of Ca-Mnt (Figure 1b). The entire peak for the Ca-Mnt fractogram shifted to ~40 min, suggesting a slight increase in size and mass. The swelling kinetics for smectite-type clays are often referred to in the literature in terms of 'days' (Katti *et al.*, 2001). The maximum residence time for the SdFFF experiments was ~1 h, which was assumed to be ineffectual in terms of clay swelling. Two important points need to be considered when analyzing clay-size distributions obtained from FFF experiments: (1) the diameter obtained in SdFFF is the equivalent spherical diameter, namely the diameter of a sphere having the same mass as the sample particle. This approximation should be noted when analyzing plate-like clay particles by FFF where the projected diameter (*e.g.* obtained by electron microscopy) is expected to be different, depending on the mass of the particle. (2) The employment of a stronger field can lead to a phenomenon known as the steric-entropic effect, where the particles can be lifted and eluted earlier, thus resulting in an apparently smaller particle size. The elution of plate-like particles could be affected by steric-entropic effects if the thickness of the sample cloud in the FFF channel (l value) is smaller than or comparable to the sample size (d) (Beckett and Giddings, 1997). In the present study the field strength was chosen so that the l/d remained significantly larger than the sample size throughout the experiments.

If the particles are too close to the SdFFF channel, interparticle repulsive forces could result in early elution

Table 2. Calculated bridging forces between Ca^{2+} or Na^+ ions and the surface of the montmorillonite unit cell given as the sum of the Schrödinger equation forces between individual molecules.

Ion	Surface	Bridging force (μJ/A)
Ca^{2+}	Montmorillonite	9.70
Ca^{2+}	Mg-doped montmorillonite	9.57
Na^+	Montmorillonite	5.67
Na^+	Mg-doped montmorillonite	5.51

https://doi.org/10.1346/CCMN.2015.0630604 Published online by Cambridge University Press

of the sample. For the retention time of 10 min, the λ value was ~5667 nm ($\lambda \approx t_0/6t_r = l/w$) which means that the center of mass of the sample cloud was considerably greater than the range of effective interparticle forces. The shifts in the fractograms can be attributed safely, therefore, to the change in particle mass rather than the particle−channel wall interactions.

The cumulative size distributions (Figure 2c,d) are more helpful in quantitative interpretation of the size-distribution data. For the fresh Na-Mnt sample, ~32% of the sample population showed an equivalent spherical diameter of <200 nm when injected immediately after preparation. The percentage of particles with an equivalent spherical diameter of <200 nm increased to 50% upon hydration. The Ca-Mnt sample showed very similar populations before and after hydration, however, although a small change in size was observed. These results are close to the values reported by Michot *et al*. (2004), who observed a bimodal size distribution for Wyoming Na-bentonite from transmission electron microscopy (TEM) images, with average diameters of ~75 nm and 300 nm. Similarly, two populations for a natural montmorillonite sample were reported (Cadene *et al.*, 2005) from atomic force microscopy (AFM) images, with average sizes of 60 nm and 350 nm, respectively; but the relative populations could not be quantified.

The EPM of the fractions obtained from the particle-size distribution for the Na-Mnt sample (Figure 3) showed that smaller particles carried a more positive charge and the charge reached a plateau at ~200 nm. These findings confirm the proposed hypothesis that the surface charge of smectite clay particles should be a distributed property. Considering the charging behavior of montmorillonite, the observed size-dependent charge for Na-Mnt (Figure 3) can be explained by either preferential adsorption of cations on the smaller particles and/or an increase in the charge at the edges because of an increase in the aspect ratio. Fractions were, therefore, collected along the size distribution of Na-Mnt and were analyzed by ICP-OES for elemental composition analysis.

ICP-OES analysis of Na-Mnt fractions

The signal obtained from ICP-OES can be converted to elemental concentrations using internal standards and the molar mass of the desired element. The elemental concentrations can then be compared with the UV trace. Elemental molar ratios (to Al or Si) can reveal information about whether a specific element is associated with the particle surface or is part of the clay structure (Taylor *et al.*, 1992). Molar concentration plots of Al and Si in Na-Mnt, obtained as a function of particle-size distribution (Figure 4), followed closely the UV trace, meaning that both elements were present in the structure of the sample. This was expected because Al and Si are major clay constituents.

The ratio of Si to Al (Figure 5) compared well with the theoretical proportion of 2.6 calculated from the structural formula. A larger Si/Al ratio at the larger sizes ($d \geqslant 300$ nm) could be indicative of a mineralogy change, perhaps toward micaceous particles.

The almost constant Fe/Al ratio throughout the size distribution (Figure 5) suggested association of Fe with the montmorillonite structure (rather than surface adsorption). Fe^{2+} ions can replace Al^{3+} in the octahedral sheet (van Olphen, 1963). The Mg to Al molar ratio was larger in the smaller size fractions, and remained constant for particles of >300 nm. The trend suggests the presence of Mg^{2+} both in the structure and also as an adsorbed entity (on the smaller particles).

The Ca/Al molar ratio showed a large scatter compared with those of Mg/Al and Fe/Al. The scatter can be attributed to the relatively low Ca^{2+} concentration in the clay sample and possible interferences during the ICP-OES experiments. The Ca/Al trend demonstrated a sharp decrease relative to the particle size, which suggested the association of the majority of the Ca^{2+} ions with the particle surface at particle diameters of <300 nm. Ca^{2+} can bond electrostatically to the basal surfaces to compensate for the charge deficit arising from the isomorphous substitution, or, depending on the solution pH, can be adsorbed to the broken edges of the clay particles (Johnston and Tombácz, 2002). The experiments outlined here were conducted in deionized water, but, upon mixing with water, the Na-Mnt suspension pH increased to ~8.6 and remained constant for at least 3 days (data not shown) which may suggest that cation adsorption to the broken −OH bonds at the clay particle edges would be plausible. In summary, the elemental molar ratio data suggest that the abundance of cations such as Ca^{2+} and Mg^{2+} in the smaller size fractions could be responsible for the greater positive charge observed by EPM measurements.

Particle-thickness calculations

Combining the data obtained from SdFFF and the projected area obtained from electron microscopy allows for the calculation of the average particle thickness (equation 3). The micrographs for the particles eluted at 13 min show transparent clay particles with a calculated thickness of 2.6 nm. These particles can be assumed to be primary particles as their thickness is fairly close to that of a 2:1 layer silicate monolayer (1 nm). The fraction collected at 38 min shows denser (darker) particles, with an average thickness of ~36 nm. These features are similar to those reported by Roberson *et al*. (1968) and Michot *et al.* (2004). The data imply that average particle thickness increased by a factor of 14 (Table 1) between the two populations.

The increased thickness of the second population can be indicative of an aggregated state, possibly caused by the presence of the cations on the particle surface. Such behavior was reported in early studies by Viani *et al.* (1983) who measured the interlayer spacing of several montmorillonite samples in equilibrium with 1×10^{-4} M

https://doi.org/10.1346/CCMN.2015.0630604 Published online by Cambridge University Press

NaCl and reported the co-existence of a partially expanded phase with a fully expanded phase in several montmorillonite samples. The fully expanded phase converted progressively to the partially expanded phase as the applied pressure was increased to >5 bar. A similar shift in the basal spacing of montmorillonite samples was reported by Low (1992) when the water content of the montmorillonite samples was decreased. Low (1992) explained this behavior as the free energy change in the clay-water system, where the aggregation kinetics would be determined by the height of the energy barrier. Shallower free-energy wells at aggregation would favor lower mean masses with a greater proportion of dispersed individual platelets. Data from Zhang and Low (1989) for several montmorillonite samples demonstrated that the free energy of the water-clay system decreases as the water content increases. Thus, the montmorillonite particles in the face-to-face arrangement would delaminate spontaneously in the presence of extra water.

Molecular dynamics simulations of layers of montmorillonite clays in explicit water, with either Na^+ or Ca^{2+} ions in the interlayer space, demonstrated that after a few femtoseconds the Na^+ ions left the interlayer space, while the Ca^{2+} ions bridged the layers together (see the aforementioned movie). This behavior is very similar to the Na-Mnt behavior observed after 4 days of hydration where the population of the smaller particles increased (Figure 1a) and agree with the phenomenon observed by Zhang and Low (1989).

The real swelling behavior is perhaps a combination of several complex phenomena where a mixture of Na^+

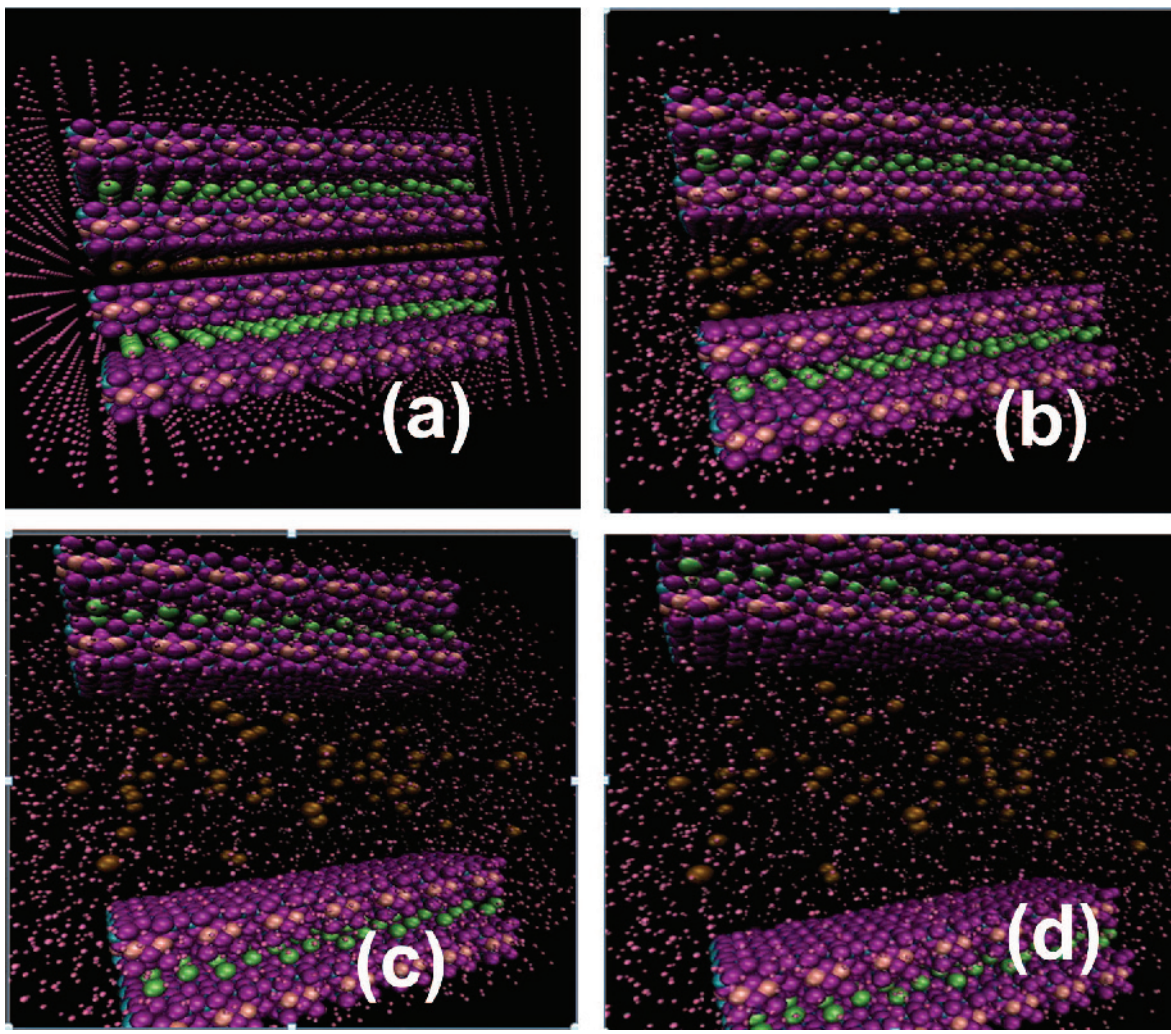

Figure 7. Snapshots from the MDS of Na-Mnt swelling (4 trilayers with alternating Na and Ca interlayer cations) The orange spheres represent Na^+ and the green spheres, Ca^{2+} ions. The shots are 40 ps apart. The progression of the swelling behavior can be observed from parts a to d. Ca^{2+} ions can hold the montmorillonite layers together, but the bridging forces between the montmorillonite and the Na^+ are not strong enough to do the same. As a result, the layers can separate and the water molecules can enter the gap and push the layers apart. (A movie is available from a file deposited with the Editor in Chief at www.clays.org/journal/JournalDeposits.html.)

https://doi.org/10.1346/CCMN.2015.0630604 Published online by Cambridge University Press

and Ca^{2+} ions exists in the interlayer, some leaving the interlayer, depending on the ionic strength of the electrolyte, and some being hydrated. This simple molecular dynamics simulation suggests that upon hydration of Na-Mnt, swelling and delamination can occur simultaneously (Figure 7). Water enters the interlayer space and the expansion only stops when the counter-pressure from the outer layers is equal to the pressure exerted by the water molecules. When the outer pressure is not sufficient, the hydration can result in the separation of the montmorillonite layers (delamination). This behavior might be different at lower pH values when the edges could bear positive charges, and will be the subject of a future investigation.

CONCLUSIONS

The first investigation of the swelling and delamination behavior of SWy-2 Na-Mnt and STx-1b Ca-Mnt using their particle-size distributions and analyses of narrow-sized clay fractions was presented here. These data and analyses demonstrate that: (1) the size distribution of sub-micron montmorillonite particles can be used as a marker to distinguish Na-Mnt from Ca-Mnt. (2) The surface charge of montmorillonite particles is not homogeneous throughout the size distribution (the bimodal size distribution of Na-Mnt observed here and reported by previous researchers can now be explained by the disparity in surface charge caused by the difference in elemental composition). (3) A 14-fold difference exists in the average particle thicknesses calculated for the two Na-Mnt populations, suggesting the coexistence of a dispersed (delaminated) and an aggregated state (Figure 8). (4) Molecular dynamics simulation provided an explanation of the delamination process. Based on these findings, delamination of the interlayers rich in monovalent cations is the source of particle swelling. The expansion of the interlayer only stops when the counter-pressure from the outer layers is equal to the pressure exerted on the particles.

Use of an elution technique (SdFFF) allowed observation of delamination and aggregation processes within a single experiment. The results demonstrated that valuable information about the swelling and delamination behavior of Na-Mnt clays can be obtained

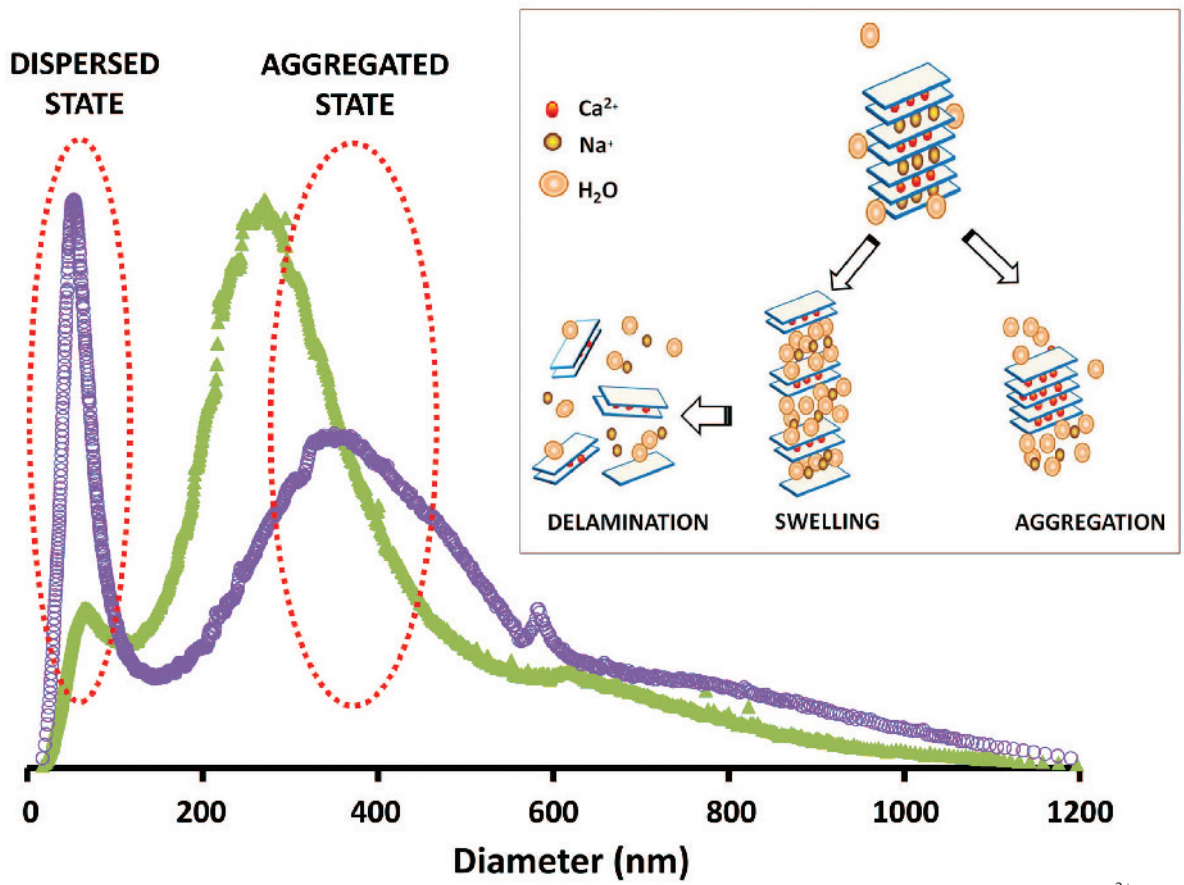

Figure 8. Schematics of the simultaneous dispersed and aggregated states observed for natural Na-Mnt containing Ca^{2+} ions. Interlayers rich in Ca^{2+} hold together and form aggregates, while interlayers rich in Na^{+} would hydrate with water, pry open, and delaminate.

https://doi.org/10.1346/CCMN.2015.0630604 Published online by Cambridge University Press

from the study of particle size at the nanometer level, and that properties such as clay charge and composition can vary with particle size.

ACKNOWLEDGMENTS

The authors are grateful to Ms Nancy Chandler for her assistance in obtaining the TEM images of the Na-Mnt fractions, to Ms Dorrie Spurlock for her assistance in preparing the manuscript and to Dr. Ronald Beckett for very helpful discussions. The authors also express their gratitude to two anonymous reviewers for their constructive comments and suggestions.

REFERENCES

Anderson, R.L., Ratcliffe, I., Greenwell, H.C., Williams, P.A., Cliffe, S., and Coveney, P.V. (2010) Clay swelling – A challenge in the oil field. *Earth Science Reviews*, **98**, 201–216.

Beckett, R. and Giddings, J.C. (1997) Entropic contribution to the retention of nonspherical particles in field-flow fractionation. *Journal of Colloid and Interface Science*, **186**, 53–59.

Beckett, R. and Hart, B.T. (1993) Use of field-flow fractionation techniques to characterize aquatic particles, colloids, and macromolecules. Pp. 165–205 in: *Environmental Particles*, *Volume 2* (J. Buffle, and H.P. van Leeuwen, editors). CRC Press, Boca Raton, Florida, USA.

Beckett, R., Nicholson, G., Hotchin, D., and Hart, B. (1992) The use of sedimentation field-flow fractionation to study suspended particulate matter. *Hydrobiologia*, **235/236**, 697–710.

Boek, E.S., Coveney, P.V., and Skipper, N.T. (1995) Monte Carlo modeling studies of hydrated Li-, Na-, K- smectites: understanding the role of potassium as a clay swelling inhibitor. *Journal of the American Chemical Society*, **117**,12608–12617.

Borden, D. and Giese, R.F. (2001) Baseline studies of The Clay Minerals Society Source Clays: Cation exchange capacity measurements by the ammonia-electrode method. *Clays and Clay Minerals*, **49**, 444–445.

Bouby, M., Geckeis, H., and Geyer, F.W. (2008) Application of asymmetric flow field-flow fractionation (AsFlFFF) coupled to inductively coupled plasma mass spectrometry (ICPMS) to the quantitative characterization of natural colloids and synthetic nanoparticles. *Analytical and Bioanalytical Chemistry*, **392**, 1447–1457.

Cadene, A., Durand-Vidal, S., Turq, P., and Brendlé, J. (2005) Study of individual Na-montmorillonite particle size, morphology, and apparent charge. *Journal of Colloid and Interface Science*, **285**, 719–730.

Chiou, C.T. and Rutherford, D.W. (1997) Effects of exchanged cation and layer charge on the sorption of water and EGME vapors on montmorillonite clays. *Clays and Clay Minerals*, **45**, 867–880.

Giddings, J.C. (1993) Field-flow fractionation: analysis of macromolecular, colloidal, and particulate materials. *Science*, **260**, 1456–1465.

Gotz, A.W., Williamson, M.J., Xu, D., Poole, D., LeGrand, S., and Walker, R.C. (2012) Routine microsecond molecular dynamic simulations with AMBER on GPUs. 1. Generalized Born. *Journal of Chemical Theory Computation*, **8**,1542–1555.

Hanwell, M.D., Curtis, D.E., Lonie, D.C., Vendermeersch, T., Zurek, E., and Hutchinson, G.R. (2012) Avogadro, an advanced semantic chemical editor, visualization and analysis platform. *Journal of Cheminformatics*, **4**, 17.

Hendricks, S.B., Nelson, R.A., and Alexander, L.T. (1940) Hydration mechanism of the clay mineral montmorillonite saturated with various cations. *Journal of the American Chemical Society*, **62**,12608–12617.

Johnston, C.T. and Tombácz, E. (2002) Surface chemistry of soil minerals. Pp. 37–67 in: *Soil Mineralogy with Environmental Applications* (J.B. Dixon and D.G. Schulze, editors). Soil Science Society of America, Madison, Wisconsin, USA.

Katti, D. and Shanmugasundaram, V.(2001) Influence of swelling on the microstructure of expansive clays. *Canadian Geotechnology Journal*, **38**, 175–182.

Laird, D.A. (1999) Layer charge influences on the hydration of expandable 2:1 phylosilicates. *Clay and Clay Minerals*, **46**, 630–636.

Laird, D.A. (2006) Influence of layer charge on the swelling of smectites. *Applied Clay Science*, **34**, 74–87.

Liu, J., Sandaklie-Nikolova, L., Wang, X., and Miller, J.D. (2014) Surface force measurements at kaolinite edge surfaces using atomic force microscopy. *Journal of Colloid and Interface Science*, **420**, 35–40.

Low, P.F. (1980) The swelling of clay: II. Montmorillonites. *Soil Science Society of America Journal*, **44**, 667–676.

Low, P.F. (1992) Interparticle forces in clay suspensions: Flocculation, viscous flow and swelling. Pp. 158–190 in: *Clay-Water Interface and its Rheological Implications* (N. Güven and R.M. Pollastro, editors). CMS Workshop Lectures, The Clay Minerals Society, Boulder, Colorado, USA.

Mermut, A.R. and Cano, A.F. (2001) Baseline studies of The Clay Minerals Society Source Clays: chemical analyses of major elements. *Clays and Clay Minerals*, **49**, 381–386.

Michot, L.J., Bihannic, I., Porsch, K., Maddi, S., Baravian, C., Mougel, J., and Levitz, P. (2004) Phase diagrams of Wyoming Na-montmorillonite clay. Influence of particle anisotropy. *Langmuir*, **20**, 10829–10837.

Norrish, K. (1954) The swelling of montmorillonite. *Discussions of the Faraday Society*, **18**, 120–134.

Novik, K.E. (2000) *Amber2lammps.py*: convert Amber files to lammps files.

Plaschke, M., Schafer, T., Bundschuh, T., Ngo Manh, T., Knopp, R., Geckeis, H., and Kim, J.I. (2001) Size characterization of bentonite colloids by different methods. *Analytical Chemistry*, **73**, 4338–4347.

Plimpton, S. (1995) Fast parallel algorithms for short-range molecular dynamics. *Journal of Computational Physics*, **117**, 1–19.

Ranville, J.F., Chittleborough, D.J., and Beckett, R. (2005) Particle-size and element distributions of soil colloids. *Soil Science Society of America Journal*, **69**, 1173–1184.

Roberson, H.E., Weir, A.H., and Woods, R.D. (1968) Morphology of particles in size-fractionated Na-montmorillonites. *Clays and Clay Minerals*, **16**, 239–247.

Schneider, C.A., Rasband, W.S., and Eliceiri, K.W. (2012) NIH Image to ImageJ: 25 years of image analysis. *Nature Methods*, **9**(7), 671–675.

Stewart, J.J.P. (2012) *MOPAC2012*. Stewart Computational Chemistry, Colorado Springs, Colorado, USA.

Tadjiki, S., Assemi, S., Deering, C., Veranth, J.M., and Miller, J.D. (2009) Detection, separation, and quantification of unlabeled silica nanoparticles in biological media using sedimentation field-flow fractionation. *Journal of Nanoparticle Research*, **11**, 981–988.

Taylor, H.E., Garbarino, J.R., Murphy, D.M., and Beckett, R. (1992) Inductively coupled plasma-mass spectrometry as an element-specific detector for field-flow fractionation particle separation. *Analytical Chemistry*, **64**, 2036–2041.

v.d. Kammer, F., Baborowski, F.M., Tadjiki, S., and Tümpling Jr., W.V. (2004) Colloidal particles in sediment pore waters:

Particle-size distributions and associated element size distribution in anoxic and re-oxidized samples, obtained by FFF-ICP-MS coupling. *Acta Hydrochimica et Hydrobiologica*, **31**, 400–410.

van Olphen, H. (1963) *An Introduction to Clay Colloid Chemistry*. Interscience Publishers, New York.

Viani, B.E., Low, P.F., and Roth, C.B. (1983) Direct measurement of the relation between interlayer force and interlayer distance in the swelling of montmorillonite. *Journal of Colloid and Interface Science*, **96**, 229–239.

Williams, P.S., Giddings, M.C., and Giddings, J.C. (2001) A data analysis algorithm for programmed Field-Flow Fractionation. *Analytical Chemistry*, **73**, 4204–4211.

Zhang, Z.Z. and Low, P.F. (1989) Relation between the heat of immersion and the initial water content of Li-, Na-, and K-montmorillonite *Journal of Colloid and Interface Science*, **133**, 461–472.

(*Received 20 June 2015; revised 24 December 2015; Ms. 1013; AE: R.J. Pruett*)